ORIGINAL ARTICLE

Simultaneous non-steroidal anti-inflammatory drug electrodetection on nitrogen doped carbon nanodots and nanosized cobalt phthallocyanine conjugate modified glassy carbon electrode

Nyaradzai Dondo [a], Munyaradzi Shumba [a], Mambo Moyo [a], Stephen Nyoni [b],*

[a] *Midlands State University, Department of Chemical Technology, P. Bag 9055, Senga Road, Gweru, Zimbabwe*
[b] *Chinhoyi University of Technology, Chemistry Department, P. Bag 7724, Chinhoyi, Zimbabwe*

Abstract Nitrogen doped carbon nanodots (NDCNDs) and nanosized cobalt tetra aminophenoxy phthalocyanines (CoTAPhPcNPs) modified glassy carbon electrodes have been successfully used in the simultaneous detection of aspirin (ASA), ibuprofen (IBU) and indomethacin (INDO). Scanning electron microscopy (SEM), transmission electron microscopy (TEM), UV–Vis spectroscopy, Fourier transform infrared spectroscopy (FTIR), cyclic voltammetry (CV) and electrochemical impedance spectroscopy (EIS) were used to probe the nature of the synthesized nanomaterials. Sequential deposition of the nanomaterials on the glassy carbon electrode yielded CoTAPhPcNPs-NDCNDs-GCE with remarkable electrocatalytic performance. Electro-oxidation of the drugs at the electrode surface was first order. This work demonstrates the synergic effect of the two nanomaterials towards simultaneous electrocatalytic detection of the drugs. Superior detection limits of ASA, IBU and INDO being 9.66×10^{-9} M, 4.19×10^{-9} M and 7.2×10^{-9} M, respectively, were obtained using differential pulse voltammetry. The developed sensor could detect two of the three (ibuprofen and indomethacin) simultaneously at significantly different potentials and exhibited remarkable reproducibility after a regeneration step.
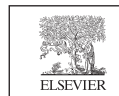
1. Introduction

Non steroidal anti-inflammatory drugs (NSAIDs) are a class of drugs that have found vast applications as analgesic agents to reduce inflammation in humans especially after cataract surgery (Nigović et al., 2018) as well as in the veterinary field and they may cause heart attack or even failure (Karimi-Maleh et al., 2018) if excessively used. The wide spread demand for

using these drugs has pushed for their voluminous production resulting in pollution of aquatic environments (Liu et al., 2018; Li et al., 2018). Recent studies have linked increased mortality of gyps vultures to excessive levels of NSAIDs such as diclophenic and ibuprofen emanating from their illegal use for veterinary purposes (Naidoo et al., 2010). This calls for the need to monitor environmental and in vivo levels of NSAIDs hence development of a robust and sensitive sensing platform is of great significance.

Carbon nanodots, a new zero dimension carbon based nanomaterial has recently shown promising electrochemical and photoluminescence (Strauss et al., 2014; Miao et al., 2015; Li et al., 2012; Zhang et al., 2012; Wu et al., 2017) properties. Very little has been reported about the use of these materials on electrocatalysis though a lot has been done with other classes such as graphene nanosheets, multiwalled carbon nanotubes (Arvand et al., 2012; Alizadeh et al., 2019) and single walled carbon nanotubes. On the other hand, metallophthalocyanines (MPcs) have been exploited for electrocatalytic detection of analytes such as hydrogen peroxide (Hosu et al., 2015; Shumba and Nyokong, 2016), nitrite (Lin et al., 2010; Maringa et al., 2014), hydrazine (O'Donoghue et al., 2016) and L-cysteine (Devasenathipathy et al., 2015; Gutierrez et al., 2012) among other analytes. A number of carbon nanomaterials have been used in combination with MPcs with outstanding catalytic properties examples of which are multiwalled carbon nanotubes (Cagrı Ceylan, 2018). The combination of these nanomaterials towards electrocatalysis in general has not been reported before.

We therefore report for the first time, the effect of carbon nanodots on the electrocatalytic behaviour of nanosized metal phthalocyanines (MPcNPs). The effect of nitrogen doped carbon nanodots (NDCNDs) on the electrocatalytic behaviour of the nanosized MPc will also be evaluated. Doped carbon based nanomaterials have shown great potential in reducing detection overpotentials and increase detection currents due to the creation of either an extra electron or hole triggering a driving force to electrical conductivity (Martínez-Periñán et al., 2018). The choice of this combination has been greatly influenced by ubiquitous availability of carbon sources and the electrocatalytic performance of CND in particular (Martínez-Periñán et al., 2018; Zhao et al., 2015) coupled with the excellent catalytic performance of MPcs. We have earlier on demonstrated that nanosizing phthalocyanines improve the electrocatalytic behaviour of MPcs (Shumba and Nyokong, 2016; Shumba and Nyokong, 2016), hence nanoparticles of cobalt tetra aminophenoxy phthalocyanine (CoTAPhPcNPs) are employed in this work. Cobalt (II) is employed as a central metal ion due to the well-known electrocatalytic activity of CoPc derivatives. The aminophenoxy substituents were employed since their bulky nature discourages aggregation which normally is a drawback in the use of MPcs for different applications. To the best of our knowledge, we present for the first time an attempt to develop a simultaneous sensing platform for the three drugs. We have in the recent times concentrated our efforts in developing sensor platforms capable of selectively detecting analytes likely to be found together simultaneously (Chihava et al., 2020; Apath et al., 2020). The beauty of such sensor platforms is that analyte determination can be done with minimum sample preparation and carbon based

nanomaterials have found vast applications in this area (Koçak et al., 2018).

2. Experimental

2.1. Materials

All chemicals were used without further purification. The following chemicals were purchased from Associated Chemical Enterprise; Potassium ferrocyanide ($K_4[Fe(CN)_6]$), sodium hydroxide (NaOH), dimethyformamide (DMF), potassium chloride (KCl), hydrochloric acid (HCl), microcrystalline cellulose, ethylenediamine, potassium ferricyanide ($K_3[Fe(CN)_6]$), di-sodium hydrogen orthophosphate (Na_2HPO4), sodium di-hydrogen orthophosphate (NaH_2PO_4), diethyl ether, methanol, cobalt chloride and potassium bromide. Ethanol (C_2H_5OH), dichloromethane and hexane were supplied by Glassworld while ibuprofen, indomethacin and aspirin were purchased from a local pharmacy. De-ionized water was prepared at MSU Chemical Technology Laboratory. Cobalt tetra aminophenoxy phthalocyanine nanoparticles (CoTAPhPcNPs) were obtained by dissolving CoTAPhPc in concentrated sulphuric acid before capping it with CTAB as described before (Shumba and Nyokong, 2016).

2.2. Equipment

All the electrochemical experimental procedures were carried out using Autolab Potentiostat PGSTAT302F installed with 1.10 version NOVA software employing a conventional three electrode system at 25 °C. The three electrode system constituted of a bare glassy carbon electrode as the working electrode, a platinum wire as an auxiliary/counter electrode and silver/silver chloride (Ag/AgCl in saturated KCl) as the reference electrode. FTIR spectra were obtained using Thermoscientific Model equipped with OMNIC software. Transmission Electron Microscopy (TEM) images were obtained from a Zeiss Libra TEM 120 model operated at 90 kV. Scanning electron microscopy (SEM) images of modified glassy carbon plates (Goodfellow, UK) were obtained using a TESCAN Vega TS 5136LM Electron microscope.

2.3. Synthesis

2.3.1. Pristine and nitrogen doped carbon nanodots (CNDs and NDCNDs)

Nitrogen doped carbon nanodots were prepared as reported elsewhere with minor alterations (Wu et al., 2017). Briefly, 2.0 g of microcrystalline cellulose was added to the ethylenediamine solution (60 ml). Comparatively, 2.0 g of microcrystalline cellulose in 60 ml of water was also prepared as a blank sample. The two obtained solutions were placed in p-polyphenol-lined stainless steel autoclaves, respectively. The autoclaves were sealed and heated in an oven for 12 h at 240 °C, and then allowed to cool to room temperature. The products were centrifuged at 10 000 rpm for 10 min. The resulting suspensions containing NDCNDs and CNDs were filtered through 0.22 mm filter membranes, and then subjected to dialysis (1000 Da molecular weight cut off) for about 72 h.

2.4. Electrode modifications

A three electrode system was used with glassy carbon electrode (GCE) as the working electrode, the silver|silver chloride (saturated potassium chloride) as the reference electrode and platinum wire as the counter electrode. Buehler-felt pad and alumina (0.05 μm) were used to polish the GCE. Deionised water was used to remove any impurities by sonicating for 5 min after each polishing step before rinsing the electrode with dionized water. The GCE was modified via the drop dry method. An optimised aliquot of 0.5 μL of 1 mg/ml of each of CNDs, NDCNDs and CoTAPhPcNPs were used as electrode modifiers to give CNDs-GCE, NDCNDs-GCE and CoTAPhPcNPs-GCE respectively. A subsequent equal amount of CoTAPhPcNPs was then added to CNDs-GCE and NDCNDs-GCE to give CoTAPhPcNPs-CNDs-GCE and CoTAPhPcNPs-NDCNDs-GCE, respectively. The modified electrodes were dried in an oven at 70 °C before use. CoTAPhPcNPs were placed on top of electrodes since we have shown before that the electrocatalytic activity of the MPcs is higher when placed on top of the nanomaterials (Maringa and Nyokong, 2014). A complete list of the electrodes is shown in **Table S1**.

3. Results and discussions

3.1. Characterization of carbon nanomaterials and their conjugates with CoTAPhPcNPs.

3.1.1. Fourier transform infrared spectra

FTIR helps to confirm the functionalities on the different electrode modifiers. The spectra of the different modifiers used in this work are shown in **Fig S1**. The peak at 1672 cm^{-1} for CNDs can be attributed to C = O stretching vibration. CNDs consist of various functional groups like COOH, OH and N-H. The characteristic absorption band of N-H (3424 cm^{-1}) and the aromatic C-N heterocycles stretching vibrations at 1420 cm^{-1} can be observed for NDCNDs. Moreover, there is a good signal of aromatic C = C stretching at 1624 cm^{-1} to 1685 cm^{-1} which indicates the presence of an sp^2 hybridized honeycomb lattice (Usai et al., 2019). Therefore, the prepared NDCNDs exhibit the distinctive sp^2 graphitic structure. The nitrogen doped carbon nanodots with various oxygen and nitrogen related groups consist of carbonyl, carboxyl, amide, ether and C-O groups. CoTAPhPc spectrum has been reported before (Shumba and Nyokong, 2016). The spectrum for CoTAPhPcNPs/CNDs shows N–H stretching of amino groups. The peak at 1672 cm^{-1} can be attributed to C=O stretching vibration. Functional groups like COOH, OH and N-H for CoTAPhPcNPs/CNDs were present. CoTAPhPcNPs/NDCNDs reveal the presence of various oxygen and nitrogen related groups in carbonyl, carboxyl, amide and C-O groups.

3.1.2. TEM images

Both Nanosized MPcs and the different forms of carbon nanodots showed monodispersed particles as seen under TEM (Fig. 1). The bigger isolated black spots in the figure may be due to minor flaws in the nanosizing step or aggregation of the monodispersed nanoparticles (Fig. 1A). Nanosized MPc appeared to be nonspherical unlike the carbon nanodots (Fig. 1B).The average size of the MPc nanoparticles was 14 nm as reported before (Shumba and Nyokong, 2016) while that of the nanodots was half the size (7 nm) as shown in the corresponding histograms showing size distribution. Carbon nanodots are zero dimension nanoparticles of size less than 10 nm (Li et al., 2012) and the TEM images confirm the same size range.

3.1.3. UV–Vis spectra

Following the formation of nanoparticles for CoTAPhPcNPs, there was no significant change in the Q band, except for the narrowing of the peak (**Figure not shown**), showing stability of the complex to the acid environment. The UV–Vis spectra of NDCNDs show the characteristic absorption band below 300 nm as observed elsewhere (Lu et al., 2017).

3.2. Characterization of modified electrodes

3.2.1. SEM images

Glassy carbon plates were viewed under a scanning electron microscope before modification (Fig. 2A) and after modification (Fig. 2B and C). The scanning electron microscope images revealed effective electrode modification characterised by different extents of surface roughness. CoTAPhPcNPs modified GCP showed cylindrically shaped nanomaterials covering the surface indicative of 'J' aggregation (Mallik and Karan, 2007) also confirming the nonspherical shape observed under transmission electron microscopy (Fig. 2B). CNDs modified carbon plate shows an array of spherical (bolus) nanomaterials covering the surface (Fig. 2C) as observed elsewhere (Hu et al., 2017).

3.2.2. Electrochemical characterisation

Fe^{2+}/Fe^{3+} system is a very good redox media and hence 1 mM [Fe(CN)$_6$]$^{3-/4-}$ in 0.1 M KCl electrolyte was employed to investigate electron transfer abilities at the surface of the modified electrode. Cyclic voltammetry and electrochemical impedance spectroscopy techniques were used for this purpose. Assuming uniform ohmic drop for all voltammetric runs for differently modified electrodes in this media, the anodic and cathodic peak separation is a good indicator for electron transferability, hence catalytic performance of the sensing platform. Such catalytic performance can be confirmed by lower charge transfer resistance (R$_{CT}$) during electrochemical impedance spectroscopy studies. Different modifications resulted in varying peak potential separations indicative of different electron transfer abilities. Lower peak potential separation (ΔE) and R$_{CT}$ in cyclic voltammetry and electrochemical impedance spectroscopy respectively, imply good electron transfer ability. Similar trends were observed from both techniques showing consistency in the performance of the fabricated probes. The inclusion of carbon nanomaterials resulted in higher redox currents implying they promote the electron transfer and improve the conductivity of the electrode (Wu et al., 2020). We therefore discuss the nature of the sensing platforms using the EIS results (**Table S1; Fig. S2**). R$_{CT}$ values may range from a few ohms for very fast reaction kinetics to greater than 10 GΩ for very slow reaction kinetics at the electrode surface (Nyoni et al., 2014). The Randles equivalent circuit that fits to the experimental data performs complex nonlinear
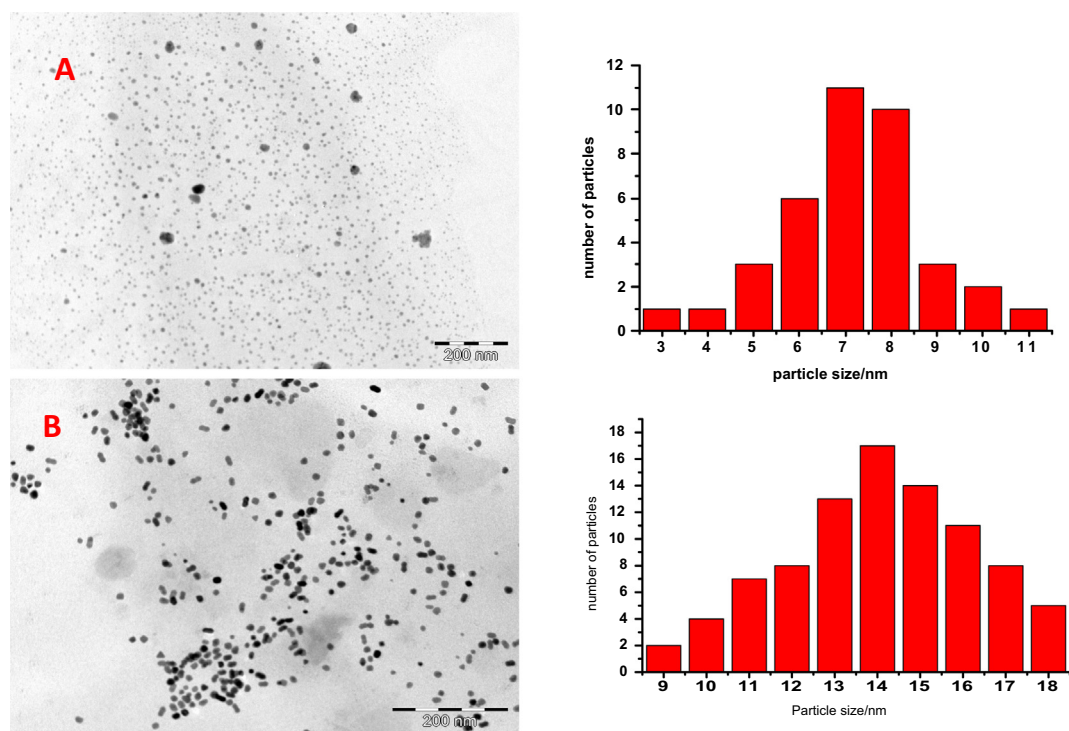
Fig. 1 TEM images of NDCNDs (A) and CoTAPhPcNPs (B) with the corresponding size distributions (histograms) alongside.
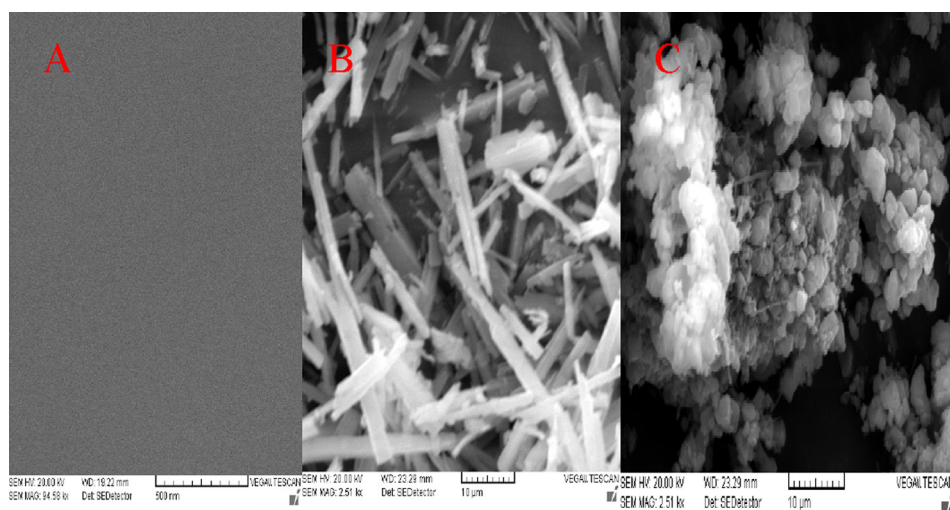

Fig. 2 SEM images for Bare GCE (A) CoTAPhPcNP-GCE (B) NDCNDs-GCE (C).

least-squares procedures available in EIS data fitting computer programme and informs on that basis to the catalytic performance of relative electrode surfaces. The corresponding Bode plots show significant phase shifts for different modifications which might imply different electrochemical behaviour in agreement with the different apparent rate constants shown in **Table S1**. Apparent electron transfer rate constants (k_{app}) were determined as reported before (Nyoni et al., 2014), using Eq. (1) , for the different electrode surfaces towards redox of $[Fe(CN)_6]^{3-/4-}$ system to confirm CV data .

$$k_{app} = \frac{RT}{F^2 A R_{CT} C} \tag{1}$$

where C = $[Fe(CN)_6]^{3-/4-}$ which is 1 mM $[Fe(CN)_6]^{3-/4-}$ and A = surface area in cm^2 obtained via the Randles Sevcic Eq. (2), with R, T and F taking their normal scientific meaning. The apparent rate constants increase in the order CNDs-GCE (1.44×10^{-7}) < NDCNDs-GCE (2.94×10^{-7}) < CoTAPhPcNP-GCE (3.63×10^{-7}) < CoTAPhPcNP-CNDs-GCE (13.3×10^{-7}) < CoTAPhPcNP-NDCNDs-GCE (14.3×10^{-7}). In general, the experimental observations show the presence of MPc improves the electron transfer ability hence lower R_{CT} values and that the conjugates perform better than the individual nanomaterials. Compare CNDs-GCE (22.60 kΩ) and NDCNDs-GCE (9.14 kΩ) with

CoTAPhPcNPs-GCE (5.61 kΩ). Also compareCoTAPhPcNPs-GCE (5.61 kΩ), to CoTAPhPcNPs-CNDs-GCE (1.15 kΩ) and CoTAPhPcNPs-NDCNDs-GCE (1.36 kΩ). This further confirms our earlier reported observations that the central metal is responsible for significant contribution towards electro catalytic redox reactions at the surface of the working electrode (Shumba and Nyokong, 2016; Shumba and Nyokong, 2016). Comparing CoTAPhPcNPs-CNDs-GCE (1.15 kΩ) to CoTAPhPcNPs-NDCNDs-GCE (1.36 kΩ) shows the advantage of introducing an impurity in the sp^2 carbon honeycomb which breaks the electro neutrality.

It is also noteworthy that modification of the bare resulted in the shift of both oxidation and reduction potentials (Fig S2A) manifesting lower activation energy involved in the presence of the catalysts. The Randles-Sevcik relation, (Eq. (2)) was applied on the cyclic voltammetric results to deduce the effective electroactive electrode surface area (Bard and Faulkner, 2001).

$$I_p = 2.69 \times 10^5 n^{3/2} ACD^{1/2} v^{1/2} \qquad (2)$$

where I_p, n, A, C, D and v are the peak current, the number of electrons involved, the surface area, the concentration of [Fe$(CN)_6]^{3-/4-}$, the diffusion coefficient of [Fe$(CN)_6]^{3-/4-}$ and the scan rate, respectively. The diffusion coefficient for K_3[Fe$(CN)_6]$ (D = 7.6×10^{-6} cm^2 s^{-1}) (Gooding et al., 1998) and n = 1 for Fe$^{2+/3+}$ redox system, was used to determine the surface roughness factors (ratio of $I_{pa\ experimental}/I_{pa\ theoretical}$) of the modified electrodes. The geometrical surface area of the bare GCE (0.071 cm^2) and the roughness factor of the modified glassy carbon electrode were then used to deduce the modified electrode effective surface area. These observations point out to a significant increase in effective electrode area upon modification by the different nanomaterials under study.

For nanosizedphthalocyanine based electrodes, cyclic voltammetry was run in pH 6 buffer, TableS1, since they had shown superior electron transfer capabilities. Ring based redox couple was observed at high potentials around 0.8 V. The effective electrode areas and the charge Q, obtained from this couple were then used to determine the surface coverage according to Eq. (3) (Bard and Faulkner, 2001).

$$\Gamma = \frac{Q}{nFA} \qquad (3)$$

where Γ is the surface coverage, n is the number of transferred electrons, F is the Faraday constant, and A is the effective area of the electrode area. Very high surface coverages were reported for the conjugates (4.27×10^{-8} mol.cm^{-2}for CoTAPhPcNP-CNDs-GCE and 3.8×10^{-8} mol.cm^{-2} for CoTAPhPcNP-NDCNDs-GCE) while that for CoTAPhPcNP-GCE (9.70×10^{-10} mol cm^{-2}) was closer to 1×10^{-10} mol.cm^{-2} reported for phthalocyanine lying flat on the surface of the electrode (Li et al., 2001) suggesting that the underlying cabonanodots moieties disrupt the metallophthalocyanines from lying parallel to the electrode surface. We have reported similar results for covalently linked metallophthalocyanines to cabon nanotubes (Shumba and Nyokong, 2017) and metallophthalocyanines doped graphene, gold nanoparticles conjugates. The higher surface coverages indicate increase in the electrode surface area which offers more electrocatalytic surface.

3.3. NSAIDs detection

3.3.1. Detection of NSAIDs

We report a number of electrochemical techniques that have been successfully explored in the detection of NSAIDs on the surface of nanosized MPcs carbon nanodots conjugate based electrodes. These include cyclic voltammetry, differential pulse voltammetry, linear sweep voltammetry, chronoamperometry and electrochemical impedance spectroscopy. Optimisation of pH was done before successful detection Fig. S3. The drugs were detected at different pHs, ASA (4), INDO (6) and IBU (5) (Table S1). The nanoprobes developed in this work are characterised by electrooxidation of ASA, IBU and INDO at 0.815 V, 1.318 V and 1.003 V, respectively, with respect to cyclic voltammetry using CoTAPhPcNP-NDCNDs-GCE as an example as it gave the best response (Fig. 3; Table S1). The detection background corrected currents on all CoTAPhPcNP based platforms were impressively high with respect to all voltammetric techniques. All the other voltammetric techniques had the same detection potentials on CoTAPhPcNP-NDCNDs-GCE confirming successful fabrication of a robust sensor platform. The same trend was observed with respect to electrochemical impedance ASA (1.33kΩ), IBU (1.27 kΩ) and INDO (1.36 kΩ) on CoTAPhPcNP-NDCNDs-GCE for the same reason given under cyclic voltammetry. The rest of the CoTAPhPcNP based nanoprobes is given in Table S1.

3.3.2. Kinetic studies of NSAIDs detection

Variation of current and detection potential during cyclic voltammetry at different scan rates using CoTAPhPcNP-NDCNDs-GCE since it is the best performing electrode was investigated to evaluate the reversibility of the electrooxidation reaction, Fig S4. The shift on the peak potential observed is evidence for an irreversible reaction on the electrode surface. Irreversible reactions are governed by Eq. (4) (Karimi-Maleh et al., 2018; Salimi and Abdi, 2004).

$$E_p = \frac{b}{2} \log v + K \qquad (4)$$

where b is the Tafel slope.

Plots of $E_p$vs log v are shown in Fig. S4. The abnormally high Tafel slopes (above the normal 60–120 mV decade^{-1}) are suggestive of chemical complication whereby the electrocatalytic reaction is followed by adsorption of intermediates or products on the electrode surface (Zen et al., 2000; Lyons et al., 1994). Such complication is usually evidenced by electrode fouling as demonstrated in Fig S5. The values of the Tafel slopes on CoTAPhPcNP-NDCNDs-GCEvaried in the order; ASA (150 mV/decade) < IBU (232 mV/decade) < INDO (196 mV/decade). High Tafel slopes may be an indication that the reaction is proceeding at a very high speed such that the rate of the products leaving the electrode surface becomes the rate determining step. This is evidenced by the plots of the square root of scan rates against currents which displayed a linear relationship showing that the reaction is diffusion controlled, Fig. S5. Diffusion controlled reactions are facile in their nature and this is expected of an efficiently catalysed reaction. The gradient of such plots can therefore be used as a measure of efficiency of the catalyst. Very high gradients were recorded indicative of a very facile electrodetection process
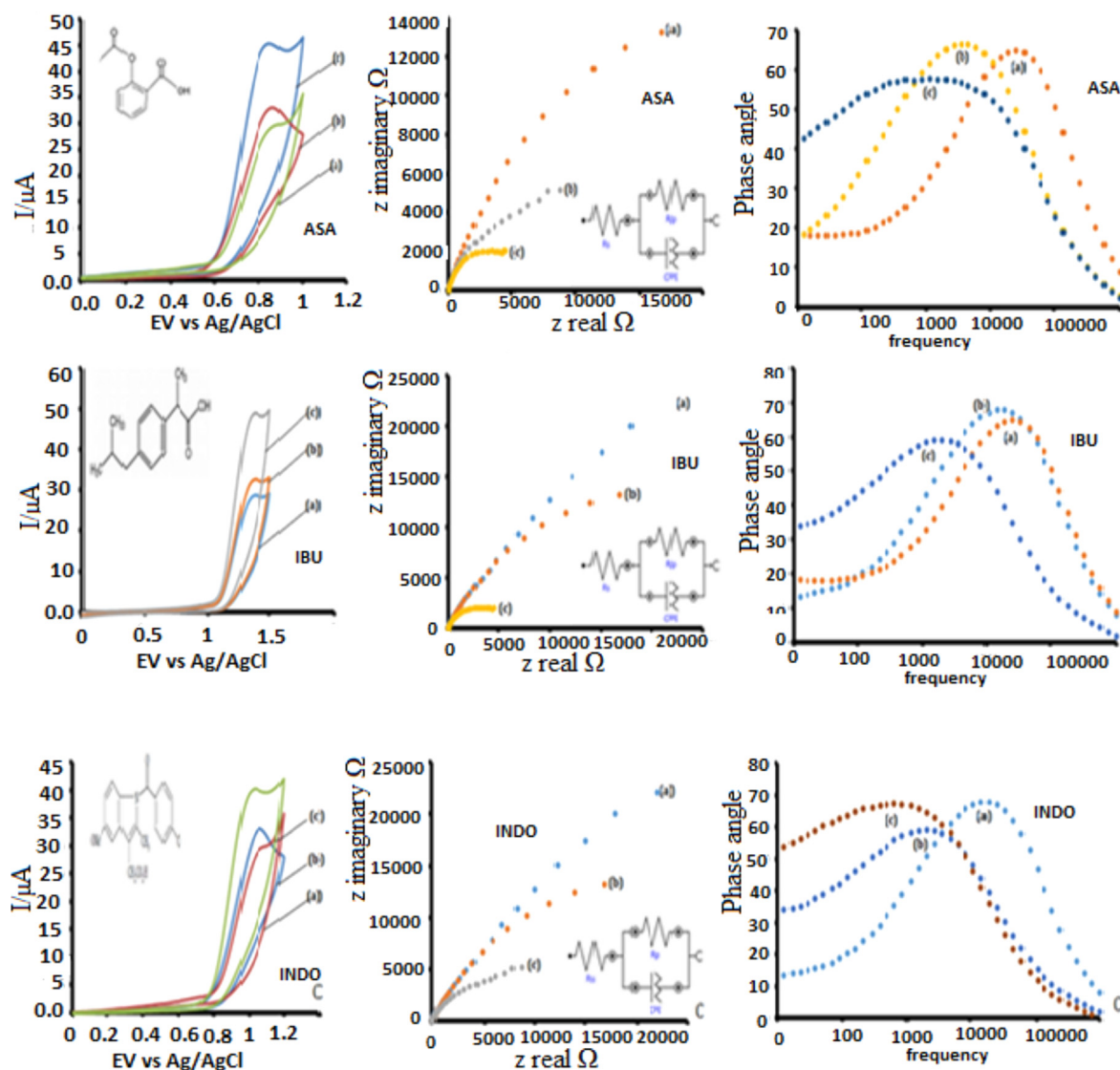
Fig. 3 CVs, Nyquist plots and Bode plots for ASA, IBU and INDO, (a) CoTAPshPcNPs-GCE, (b) CoTAPhPcNPs-CNDs-GCE, (c)) CoTAPhPcNPs-NDCNDs-GCE.

which increase in the order (units = $\mu A/(mV.s^{-1})^o$; IBU (10) < INDO (30) = ASA (30).

Langmuir adsorption theory helps explain the adsorptive nature of heterocatalytic surfaces such as modified electrode surfaces. The abnormally high Tafel slopes coupled with significant electrode surface fouling, linear sweep voltammetry (Fig. S6) was done for the detection of the three drugs under study on anodic reaction of CoTAPhPcNP-NDCNDs-GCE since it was the best performing electrode in order to understand the adsorptive behaviour during the catalytic detection. Linear plots of the ratio of drug concentration to catalytic current against concentration of the different drugs under study was obtained (Fig. S6, Equation5 (Adekunle et al., 2011).

$$\frac{[H_2O_2]}{I_{cat}} = \frac{1}{\beta I_{max}} + \frac{[H_2O_2]}{I_{max}} \quad (5)$$

where β is the adsorption equilibrium constant, I_{max} is the theoretical maximum current and I_{cat} is the catalytic current. Langmuir adsorption equilibrium constant (β) was found to

be 1.05×10^5 M^{-1}, 1.2×10^5 M^{-1} and 5.56×10^5 M^{-1} for ASA, IBU and INDO respectively. These equilibrium constants culminate to Gibbs energy changes (ΔG^o) (using Eq. (6)) due to adsorption of values-28.63 kJ mol^{-1}, -28.96 kJ mol^{-1} and -27.07 kJ mol^{-1}for ASA, IBU and INDO respectively. Such high Gibbs energy changes point out to a thermodynamically spontaneous reactions (Adekunle et al., 2011) hence favouring the possibility of transforming the fabricated nanoprobe into a practical solution to the detection of the drugs under study.

$$\Delta G^o = -RT \ln\beta \quad (6)$$

where R is the molar gas constant and T is room temperature.

3.3.3. LODs and catalytic rate constants for NSAIDs

Limits of detection were investigated using differential potential voltammetry while catalytic rate constants were determined by chronoamperometry. The values reported here for the LODs are comparable and even better that those reported

elsewhere making the probes in this work a promising platform for the NSAIDs detection (**Table S2**) (Karimi-Maleh et al., 2018; Liu et al., 2018).

The chonoamperometriccatalytic currents during the rapid decay period are dominated by the rate of electro-oxidation reaction of NSAIDs. The technique was used to evaluate the catalytic rate constants for the electrocatalytic oxidation of the drugs under investigation on CoTAPhPcNP-NDCNDs-GCE as shown in Fig. 4. Linear plots were obtained for the ratio of catalytic currents and buffer currents versus time (Eq. (7)) during the rapid decay time.

$$\frac{I_{cat}}{I_{buf}} = \gamma^{1/2}\pi^{1/2} = \pi^{1/2}(kCt)^{1/2} \tag{7}$$

where I_{cat} and I_{buf} are the catalytic currents in drug oxidation and corresponding pH supporting solutions, respectively, $\gamma = kCt$ (C is the bulk concentration of drug under investigation, k is the catalytic rate constant, and t is the time elapsed in seconds).

Plotting the square of the slopes forCoTAPhPcNP-NDCNDs-GCE (from Fig. 4 against the respective concentrations of corresponding drugs gave linear plots) whose slope is equal to πk where k is the rate constant. The plots are represented by equations (8A)-C

CoTAPhPcNP-NDCNDs-GCE:

$$y = 5.212[ASA]\left(\frac{s^{-1}}{mM}\right) - 2x10^{-6}s^{-1}, R^2 = 0.939 \tag{8A}$$

$$y = 4.462[IBU]\left(\frac{s^{-1}}{mM}\right) - 5x10^{-6}s^{-1}, R^2 = 0.992 \tag{8B}$$

$$y = 0.614[INDO]\left(\frac{s^{-1}}{mM}\right) + 1x10^{-8}s^{-1}, R^2 = 0.993 \tag{8C}$$

The catalytic rate constants were established to be 1.95×10^2 M^{-1} s^{-1}, 1.42×10^3 M^{-1} s^{-1} and 1.66×10^3 M^{-1} s^{-1} for ASA, IBU and INDO respectively on CoTAPhPcNP-NDCNDs-GCE indicating a facile reaction and confirming the kinetics discussed earlier.
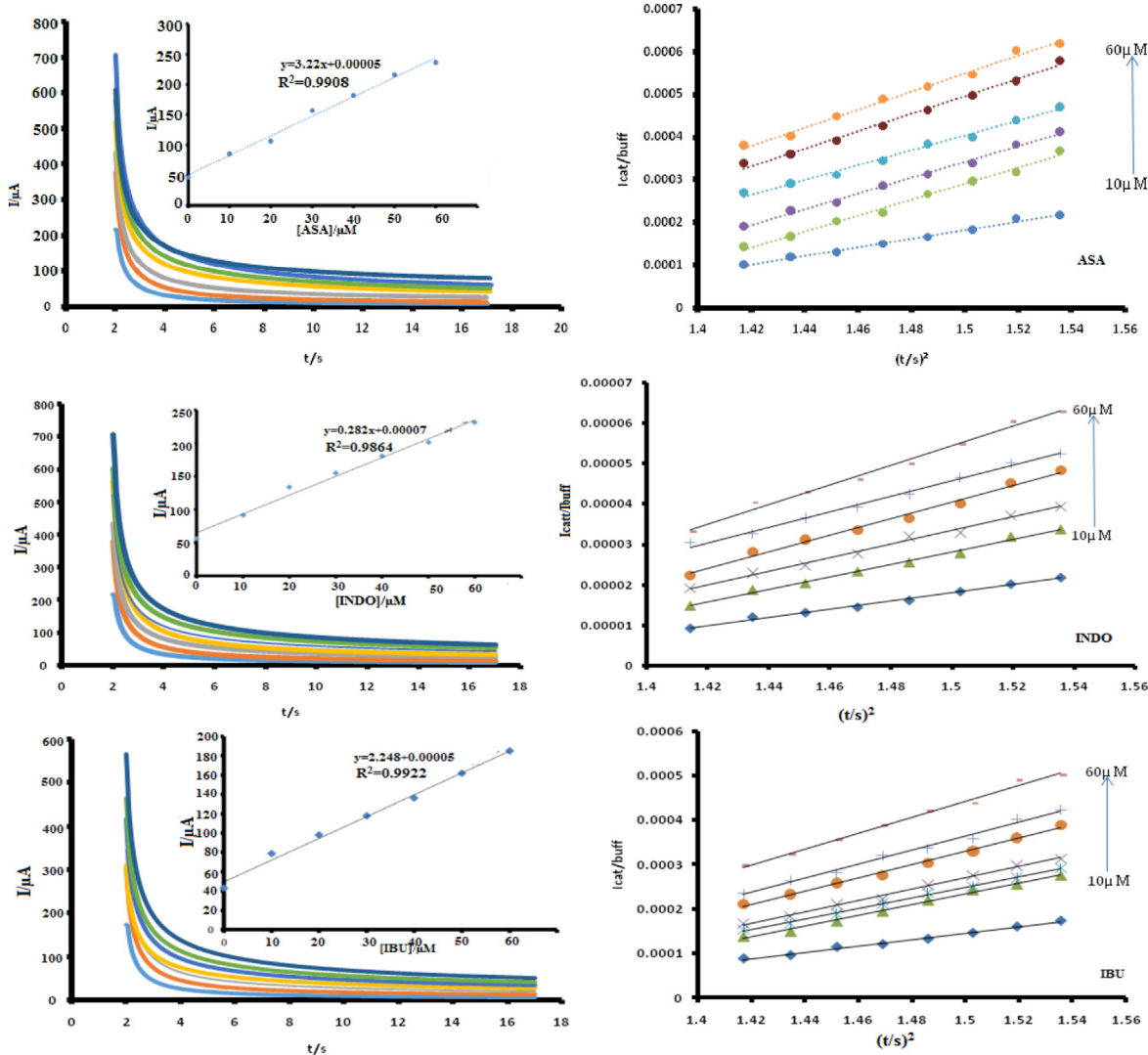

Fig. 4 Chronoamperogramms on CoTAPhPcNP-NDCNDs-GCE at different concentrations inset = corresponding calibration curve and corresponding plots of current ratio versus square root of time for NSAIDsat respective detection potentials. In PBS pH 5.5.

### 3.3.4. Practical application of developed sensor

The developed sensor was tested against a number of performance characteristics such as reproducibility, applicability in real samples and or real sample mimics. The oxidation peak resisted electrode fouling during the detection of the drugs under study {Fig S5, using CoTAPhPcNP-NDCNDs-GCE as an example}, with the peak still present even after as many scans as 20. The sensor platform could however be regenerated by simply sonicating for thirty minutes in deionized water (Fig S7). Employing the regeneration step in between measurements, the signal loss after 10 cycles for ASA, IBU and INDO on CoTAPhPcNP-NDCNDs-GCE was found to be 5.5%,

8.4% and 7.2%, respectively, confirming reproducibility of results (Fig S7).

We have of late developed interest in developing probes that can simultaneously detect more than one analyte in the same media (Bhengo et al., 2018). The probe was therefore further tested for its ability to simultaneously detect the drugs. Solutions were prepared containing ASA/IBU/INDO, ASA/IBU, IBU/INDO and ASA/INDO unimolar concentrations. In no circumstance was the probe able to pick all the three drugs. It was however possible to pick IBU/INDO in both IBU/INDO and IBU/INDO/ASA solutions by both cyclic voltammetry and differential pulse voltammetry (Fig. 5). We
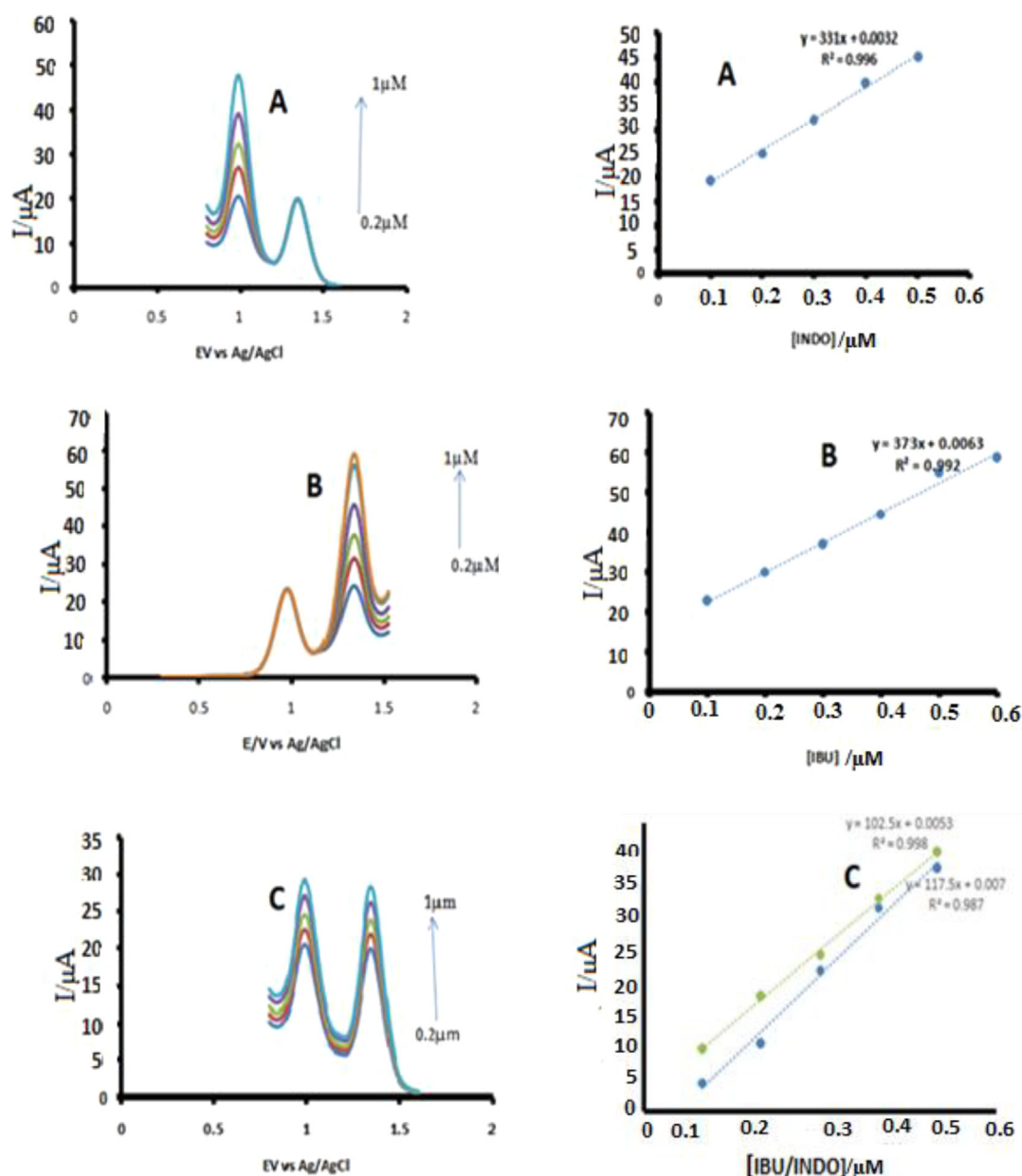
Fig. 5 DPV for CoTAPhPcNP-NDCNDs-GCE in PBS (pH 5.5) containing a mixture of A: 0.1–0.5 μM INDO, 0.2 μM IBU. B: 0.1–0.6 μM IBU, 0.2 μM INDO and C: 0.1–0.5 μM of IBU/IDO each. Insets show the relationship of Ipa versus the concentrations of each analyte.
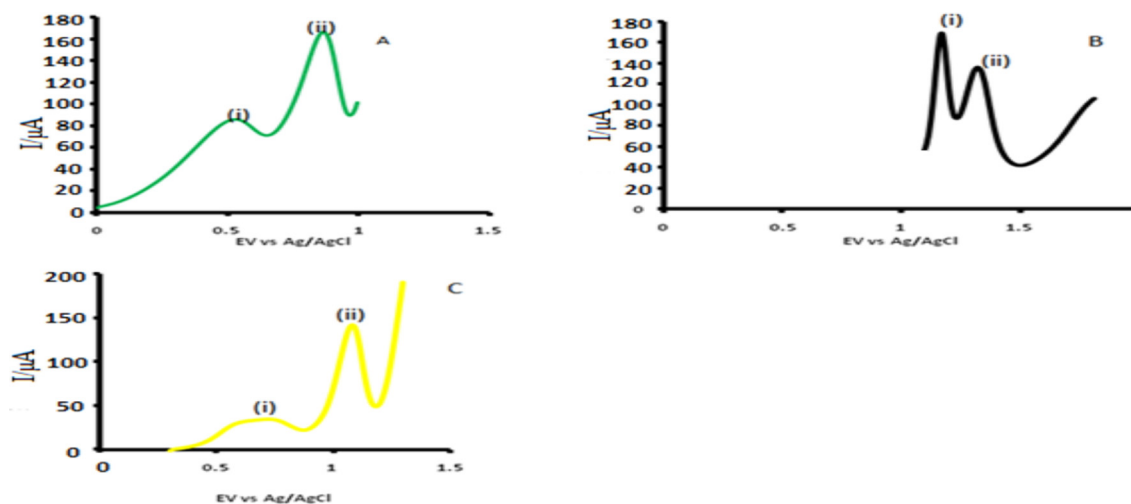
Fig. 6 DPVs for (A) (i) ascorbic acid, (ii) ASA (B) (i) citric acid, (ii) IBU and (C) (i) glucose, (ii) INDO in PBS at CoTAPhPcNPs-NDCNDs-GCE. In PBS buffer pH 5.5.

further established that the probe for IBU and INDO, the probe could linearly detect changes in one analyte concentration while the other was constant. It also could detect simultaneous changes of concentrations in the compound solutions as shown in Fig. 5.

Normally when these drugs are discharged with waste industrial waters, the matrix contains many other chemical species. In order to establish whether the developed probe would be useful in the presence of other matrices, detection was done under optimum conditions in the presence of 10 fold organic molecules such as ascorbic acid, citric acid and glucose and results are represented in Fig. 6 as reported before (Koçak et al., 2018). Waste water samples were filtered and diluted 100 fold before spiking with known amounts of the drugs under study and the amounts confirmed using the developed probe (Atta et al., 2010). The spiked samples also showed very competent recoveries, confirming the applicability of the devised probe (Table S3). Best recoveries were obtained for ASA in the range 100.4% − 101.8%, followed by IBU in the range 91.2% – 96.3% and 90.6% – 94.7% for INDO. Such recoveries are in the range of our previous work and good enough for the intended purpose. The electrodes also stability over a period of 45 days when stored under room temperature with a signal loss of less than 5% for all the analytes, far much better than values recorded elsewhere (He et al., 2019). The method of modification proved to be reproducible after repeated modifications (10 modified surfaces) on clean surfaces varied in signal within 2%

4. Conclusions

Nitrogen doped carbon nanodots and cobalt based phthalocyanine conjugate modified glassy carbon electrode (CoTAPhPcNP-NDCNDs-GCE) was succesfully applied towards detection of ibuprofen, indomethacin and aspirin in aqueous media. The developed platform could quantitatively detect ibuprofen and indomethacin by differential potential voltammetry and cyclic voltammetry simultaneously. Conjugates of NDCNDs and metalophthalocyanines performed better than those of pristine CNDs showing the importance of

breaking the electroneutrality via doping of cabon nanomaterials with heteroatoms. Appreciably low detection limits were recorded for all the three drugs accompanied by high catalytic rate constants. The spontaneity of the electrooxidation of the drugs was confirmed by large negative Gibbs energy values in the order -28.63 kJ mol^{-1}, -28.96 kJ mol^{-1} and -27.07 kJ mol^{-1} for ASA, IBU and INDO, respectively. The ability of the probe to detect IBU and INDO simultaneously is a great promise for a good electrocatalytic detector. Moreover, the developed sensor could be easily regenerated with minimal signal loss. Related chemical species such as citric acid, glucose and ascorbic acid had a different detection potential thereby not interfering with the detection of the drugs under study. Such performance shows that the developed nanoprobes have great potential as NSAIDs sensing platforms.

Declaration of Competing Interest

Authors declare no competing interests.

Appendix A. Supplementary material

Supplementary data to this article can be found online at https://doi.org/10.1016/j.arabjc.2020.09.012.

References

Nigović, B., Jurić, S., Mornar, A., 2018. Electrochemical determination of nepafenac topically applied nonsteroidal anti-inflammatory drug using graphene nanoplatelets-carbon nanofibers modified glassy carbon electrode. J. Electroanal. Chem. 817, 30–35.

Karimi-Maleh, H., Sheikhshoaie, I., Samadzadeh, A., 2018. Simultaneous electrochemical determination of levodopa and piroxicam using a glassy carbon electrode modified with a ZnO–Pd/CNT nanocomposite. RSC Adv. 8 (47), 26707–26712.

Liu, Y., Huang, Q., Zhang, C., Liang, C., Wei, L., Peng, J., 2018. A novel method for indomethacin determination based on graphene loaded nickel oxides nanoparticles film. Int. J. Electrochem. Sci. 13, 1484–1494. https://doi.org/10.20964/2018.02.39.

Li, R., Cai, M., Liu, H., Liu, G., Lv, W., 2018. Chemsphere thermo-activated peroxydisulfate oxidation of indomethacin: Kinetics study and in fl uences of co-existing substances. Chemosphere 212, 1067–1075. https://doi.org/10.1016/j.chemosphere.2018.08.126.

V. Naidoo, K. Wolter, D. Cromarty, M. Diekmann, N. Duncan, A.A. Meharg, M.A. Taggart, L. Venter, R. Cuthbert, V. Naidoo, K. Wolter, D. Cromarty, M. Diekmann, N. Duncan, A. Meharg, M. A. Taggart, L. Venter, R. Cuthbert, Toxicity of non-steroidal anti-inflammatory drugs to Gyps vultures : a new threat from ketoprofen Toxicity of non-steroidal anti-inflammatory drugs to Gyps vultures : a new threat from ketoprofen, (2010) 339–341. doi:10.1098/rsbl.2009.0818.

Strauss, V., Margraf, J.T., Dolle, C., Butz, B., Nacken, T.J., Walter, J., Bauer, W., Peukert, W., Spiecker, E., Clark, T., Guldi, D.M., 2014. Carbon nanodots: toward a comprehensive understanding of their photoluminescence. J. Am. Chem. Soc. 136 (49), 17308–17316.

Miao, P., Han, K., Tang, Y., Wang, B., Lin, T., Cheng, W., 2015. Recent advances in carbon nanodots: synthesis, properties and biomedical applications. Nanoscale 7 (5), 1586–1595.

Li, H., Kang, Z., Liu, Y., Lee, S.-T., 2012. Carbon nanodots: synthesis, properties and applications. J. Mater. Chem. 22 (46), 24230. https://doi.org/10.1039/c2jm34690g.

Zhang, H., Huang, H., Ming, H., Li, H., Zhang, L., Liu, Y., Kang, Z., 2012. Carbon quantum dots/Ag3PO4 complex photocatalysts with enhanced photocatalytic activity and stability under visible light. J. Mater. Chem. 22 (21), 10501. https://doi.org/10.1039/c2jm30703k.

Wu, P., Li, W., Wu, Q., Liu, Y., Liu, S., 2017. Hydrothermal synthesis of nitrogen-doped carbon quantum dots from microcrystalline cellulose for the detection of Fe 3 + ions in an acidic environment. RSC Adv. 7 (70), 44144–44153.

Arvand, M., Gholizadeh, T.M., Zanjanchi, M.A., 2012. MWCNTs/Cu (OH)2 nanoparticles/IL nanocomposite modified glassy carbon electrode as a voltammetric sensor for determination of the non-steroidal anti-inflammatory drug diclofenac. Mater. Sci. Eng., C 32 (6), 1682–1689.

Alizadeh, T., Atashi, F., Ganjali, M.R., 2019. Molecularly imprinted polymer nano-sphere/multi-walled carbon nanotube coated glassy carbon electrode as an ultra-sensitive voltammetric sensor for picomolar level determination of RDX. Talanta 194, 415–421.

Hosu, I.S., Wang, Q., Vasilescu, A., Peteu, S.F., Raditoiu, V., Railian, S., Zaitsev, V., Turcheniuk, K., Wang, Q.i., Li, M., Boukherroub, R., Szunerits, S., 2015. Cobalt phthalocyanine tetracarboxylic acid modified reduced graphene oxide: a sensitive matrix for the electrocatalytic detection of peroxynitrite and hydrogen peroxide. RSC Adv. 5 (2), 1474–1484.

Shumba, M., Nyokong, T., 2016. Characterization and electrocatalytic activity of nanocomposites consisting of nanosized cobalt tetraaminophenoxy phthalocyanine, multi-walled carbon nanotubes and gold nanoparticles. Electroanalysis 28 (7), 1478–1488.

Lin, C.-Y., Balamurugan, A., Lai, Y.-H., Ho, K.-C., 2010. A novel poly(3,4-ethylenedioxythiophene)/iron phthalocyanine/multi-wall carbon nanotubes nanocomposite with high electrocatalytic activity for nitrite oxidation. Talanta 82 (5), 1905–1911.

Maringa, A., Antunes, E., Nyokong, T., 2014. Electrochemical behaviour of gold nanoparticles and Co tetraaminophthalocyanine on glassy carbon electrode. Electrochim. Acta 121, 93–101.

O'Donoghue, C.S.J.N., Fomo, G., Nyokong, T., 2016. Electrode modification using alkyne manganese phthalocyanine and click chemistry for electrocatalysis. Electroanalysis 28 (12), 3019–3027.

Devasenathipathy, R., Mani, V., Chen, S.M., Kohilarani, K., Ramaraj, S., 2015. Determination of L-cysteine at iron tetrasulfonated phthalocyanine decorated multiwalled carbon nanotubes film modified electrode. Int. J. Electrochem. Sci. 10, 682–690.

A.P. Gutierrez, M.R. Argote, S. Griveau, J.H. Zagal, S.G. Granados, A.A. Ordas, F. Bedioui, Catalytic activity of electrode materials based on polypyrrole, multi-wall carbon nanotubes and cobalt phthalocyanine for the electrooxidation of glutathione and L-cysteine, J. Chil. Chem. Soc. 57 (2012) 1244–1247.

Z.D. Cagrı Ceylan KOCAK1, Enhanced electrocatalytic activity of copper phthalocyanine / multiwalled carbon nanotube composite electrode via Pt nanoparticle modification for oxygen, Turkish J. Chem. 42 (2018) 623–638. doi:10.3906/kim-1704-27.

Martínez-Periñán, Emiliano, Bravo, Iria, Rowley-Neale, Samuel J., Lorenzo, Encarnación, Banks, Craig E., 2018. Carbon nanodots as electrocatalysts towards the oxygen reduction reaction. Electroanalysis 30 (3), 436–444.

Zhao, Shunyan, Li, Chuanxi, Huang, Hui, Liu, Yang, Kang, Zhenhui, 2015. Carbon nanodots modified cobalt phosphate as efficient electrocatalyst for water oxidation. J. Materiomics 1 (3), 236–244.

Shumba, Munyaradzi, Nyokong, Tebello, 2016. Electrocatalytic activity of nanocomposites of sulphur doped graphene oxide and nanosized cobalt phthalocyanines. Electroanalysis 28 (12), 3009–3018.

Shumba, Munyaradzi, Nyokong, Tebello, 2016. Development of nanocomposites of phosphorus-nitrogen co-doped graphene oxide nanosheets and nanosized cobalt phthalocyanines for electrocatalysis. Electrochim. Acta 213, 529–539.

Chihava, R., Apath, D., Moyo, M., Shumba, M., Chitsa, V., 2020. One-pot synthesized nickel-cobalt sulfide-decorated graphene quantum dot composite for simultaneous electrochemical determination of antiretroviral drugs: lamivudine and tenofovir disoproxil fumarate. J. Sensors. 2020, 1–13.

Apath, Daniel, Moyo, Mambo, Shumba, Munyaradzi, 2020. TiO2 nanoparticles decorated graphene nanoribbons for voltammetric determination of an anti-HIV drug nevirapine. J. Chem. 2020, 1–13.

Koçak, Çağrı Ceylan, Nas, Asiye, Kantekin, Halit, Dursun, Zekerya, 2018. Simultaneous determination of theophylline and caffeine on novel [Tetra-(5-chloroquinolin-8-yloxy) phthalocyanato] manganese(III)-Carbon nanotubes composite electrode. Talanta 184, 452–460.

Shumba, Munyaradzi, Nyokong, Tebello, 2016. Electrode modification using nanocomposites of boron or nitrogen doped graphene oxide and cobalt (II) tetra aminophenoxy phthalocyanine nanoparticles. Electrochim. Acta 196, 457–469.

Maringa, Audacity, Nyokong, Tebello, 2014. The influence of gold nanoparticles on the electroactivity of nickel tetrasulfonated phthalocyanine. J. Porphyrins Phthalocyanines 18 (08n09), 642–651.

Usai, Vincent, Mugadza, Tawanda, Chigondo, Fidelis, Shumba, Munyaradzi, Nharingo, Tichaona, Moyo, Mambo, Tshuma, Piwai, 2019. Synthesis and characterisation of cobalt oxide nanoparticles decorated graphene oxide and its electrocatalytic behaviour. Polyhedron 157, 192–199.

Lu, Siyu, Sui, Laizhi, Liu, Junjun, Zhu, Shoujun, Chen, Anmin, Jin, Mingxing, Yang, Bai, 2017. Near-infrared photoluminescent polymer-carbon nanodots with two-photon fluorescence. Adv. Mater. 29 (15), 1603443. https://doi.org/10.1002/adma.201603443.

Mallik, B., Karan, S., 2007. Scanning electron microscopic characterization of copper (II) phthalocyanine nanocrystallites thin films deposited on technologically important substrates. Mod. Res. Educ. Top. Microsc. 1, 671–682.

Hu, Q., Gong, X., Liu, L., Choi, M.M.F., 2017. Characterization and analytical separation of fluorescent carbon nanodots. J. Nanomater. 2017, 30–37.

Wu, Yiyong, Deng, Peihong, Tian, Yaling, Ding, Ziyu, Li, Guangli, Liu, Jun, Zuberi, Zavuga, He, Quanguo, 2020. Rapid recognition

and determination of tryptophan by carbon nanotubes and molecularly imprinted polymer-modified glassy carbon electrode. Bioelectrochemistry 131, 107393. https://doi.org/10.1016/j.bioelechem.2019.107393.

Nyoni, Stephen, Mugadza, Tawanda, Nyokong, Tebello, 2014. Improved l-cysteine electrocatalysis through a sequential drop dry technique using multi-walled carbon nanotubes and cobalt tetraaminophthalocyanine conjugates. Electrochim. Acta 128, 32–40.

A.J. Bard, L.R. Faulkner, ELECTROCHEMICAL METHODS: Fundamentals and applications, 3rd ed., JOHN WILEY & SONS, INC., New York, 2001. doi:10.1146/annurev.matsci.30.1.117.

Gooding, J.J., Praig, V.G., Hall, E.A.H., 1998. Platinum-catalyzed enzyme electrodes immobilized on gold using self-assembled layers. Anal. Chem. 70 (11), 2396–2402.

Li, Z., Lieberman, M., Hill, W., 2001. XPS and SERS study of silicon phthalocyanine monolayers: Umbrella vs octopus design strategies for formation of oriented SAMs. Langmuir 17, 4887–4894. https://doi.org/10.1021/la010203g.

Shumba, Munyaradzi, Nyokong, Tebello, 2017. Effects of covalent versus non-covalent interactions on the electrocatalytic behavior of tetracarboxyphenoxyphthalocyanine in the presence of multi-walled carbon nanotubes. J. Coord. Chem. 70 (9), 1585–1600.

Salimi, Abdollah, Abdi, Kamaleddin, 2004. Enhancement of the analytical properties and catalytic activity of a nickel hexacyanoferrate modified carbon ceramic electrode prepared by two-step sol–gel technique: application to amperometric detection of hydrazine and hydroxyl amine. Talanta 63 (2), 475–483.

Zen, J.-M, Senthil Kumar, A, Chang, M.-R, 2000. Electrocatalytic oxidation and trace detection of amitrole using a Nafion/lead–ruthenium oxide pyrochlore chemically modified electrode. Electrochim. Acta 45 (10), 1691–1700.

Lyons, Michael E.G., Fitzgerald, Catherine A., Smyth, Malcolm R., 1994. Glucose oxidation at ruthenium dioxide based electrodes. Analyst 119 (5), 855. https://doi.org/10.1039/an9941900855.

Adekunle, A.S., Mamba, B.B., Agboola, B.O., Ozoemena, K.I., 2011. Nitrite Electrochemical Sensor Based on Prussian Blue/Single-Walled Carbon Nanotubes Modified Pyrolytic Graphite Electrode. Int. J. Electrochem. Sci. 6, 4388–4403 http://search.ebscohost.com/login.aspx?direct=true&profile=ehost&scope=site&authtype=crawler&jrnl=14523981&AN=67678088&h=cQeCs1xXz+hclOXSYlbFJaGn4YRV2/LnKN0XwzndyI8LO+aaMv1TuX3T5uqTyhmYRBocdG6U7HRdZJlKdo0Bxw==&crl=c.

Govindasamy, Mani, Mani, Veerappan, Chen, Shen-Ming, Maiyalagan, Thandavarayan, Selvaraj, S., Chen, Tse-Wei, Lee, Shih-Yi, Chang, Wen-Han, 2017. Highly sensitive determination of non-steroidal anti-inflammatory drug nimesulide using electrochemically reduced graphene oxide nanoribbons. RSC Adv. 7 (52), 33043–33051.

Bhengo, T., Moyo, M., Shumba, M., Okonkwo, O.J., 2018. Simultaneous oxidative determination of antibacterial drugs in aqueous solutions using an electrode modified with MWCNTs decorated with Iron Oxide nanoparticles. New J. Chem. 42. https://doi.org/10.1039/c8nj00129d.

Atta, Nada F., El-Kady, Maher F., Galal, Ahmed, 2010. Simultaneous determination of catecholamines, uric acid and ascorbic acid at physiological levels using poly(N-methylpyrrole)/Pd-nanoclusters sensor. Anal. Biochem. 400 (1), 78–88.

He, Quanguo, Liu, Jun, Liu, Xiaopeng, Li, Guangli, Chen, Dongchu, Deng, Peihong, Liang, Jing, 2019. A promising sensing platform toward dopamine using MnO2 nanowires/electro-reduced graphene oxide composites. Electrochim. Acta 296, 683–692.